

Influence of alumina content on the nucleation crystallization and microstructure of barium fluorphlogopite glass-ceramics based on $8\text{SiO}_2 \cdot Y\text{Al}_2\text{O}_3 \cdot 4\text{MgO} \cdot 2\text{MgF}_2 \cdot \text{BaO}$

Part I Nucleation and crystallization behaviour

J. HENRY

Department of Material Science and Technology, University of Limerick, Plassey Park, Limerick, Ireland

R. G. HILL

Department of Materials, Imperial College of Science, Technology and Medicine, London SW7 2BP, UK

E-mail: r.hill@ic.ac.uk

The effect of varying the aluminium oxide content on the nucleation and crystallization behaviour of barium containing glasses based on $8\text{SiO}_2 \cdot Y\text{Al}_2\text{O}_3 \cdot 4\text{MgO} \cdot 2\text{MgF}_2 \cdot \text{BaO}$ was investigated in order to develop novel, high strength, machinable glass-ceramics. Nine glasses were synthesized and characterized by Differential Scanning Calorimetry (DSC) Combined Differential Thermal Analysis Thermal Gravimetric Analysis (DTA/TGA), X-ray diffraction (XRD) and dilatometry.

The glass transition temperature (T_g) and first peak crystallization temperature (T_{p1}) reduced with reducing alumina content. Glasses with $Y > 1.5$ exhibited a second peak crystallization temperature (T_{p2}). T_{p1} was shown to correspond to the crystallization of barium fluorphlogopite ($\text{BaSi}_6\text{Al}_2\text{Mg}_6\text{F}_2\text{O}_{19}$) and T_{p2} to the crystallization of cordierite ($\text{Mg}_2\text{Al}_2\text{Si}_5\text{O}_{18}$). The thermal expansion coefficient (TEC) was insensitive to alumina content. All the glasses exhibited an optimum nucleation temperature just above T_g , which was thought to be a result of amorphous phase separation (APS). DTA/TGA showed the glasses to undergo weight loss corresponding to silicon tetrafluoride volatilization from the surface, which resulted in a fluorphlogopite deficient surface layer. © 2004 Kluwer Academic Publishers

1. Introduction

Fluormica glass-ceramics are the basis of machinable ceramics that can be turned, drilled and cut with conventional tipped tools [1–4]. Existing commercial materials are based on potassium fluorphlogopite and include Macor™ produced by Corning. The machinability of these materials is a direct result of the mica crystal structure shown in Fig. 1 and the weak bonding between the layers. Crack propagation takes place preferentially along the 001 cleavage plane. The microstructure of these machinable glass-ceramics consists of elongated mica crystals about 10 μm in length that contact on one another. The microstructure of the commercially available material Macor™ is shown in Fig. 2 and is termed the “house of cards” structure.

Despite the widespread commercial use of machinable glass-ceramics there exists very few systematic studies of how the composition of the glass influences the formation of the fluorphlogopite crystal phase.

Furthermore there are very limited studies of glass-ceramics based on alkaline earth fluorphlogopites [5, 6] and in particular barium fluorphlogopites that are claimed to have higher strength than the related potassium fluorphlogopite glass-ceramics [6].

Hoda and Beall [5] from Corning glass works in the USA undertook the first studies of the alkali earth fluormica glass-ceramics. They investigated glasses close in composition to the respective fluorphlogopite stoichiometry. Compositions were prone to crystallization during casting. Only one “off” stoichiometric composition was investigated and despite offering improved strength no further studies exist in the literature where compositional details are given. Hoda and Beall investigated barium, calcium and strontium containing compositions.

More recently Uno *et al.* [6] investigated glasses from the ternary system $\text{Ca}_3(\text{PO}_4)_2\text{-Ba}_{0.5}\text{Mg}_3(\text{Si}_3\text{AlO}_{10})\text{F}_2\text{-Mg}_2\text{Al}_4\text{Si}_5\text{O}_{18}$. No specific compositional details were

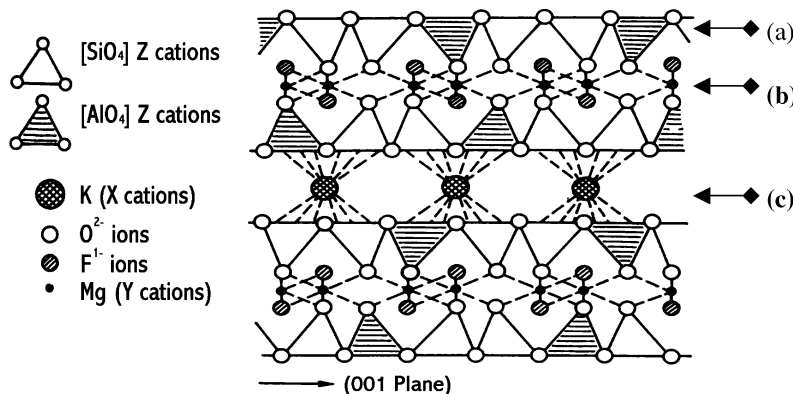


Figure 1 Schematic of the layered structure of a fluormica crystal with its hexagonal layer of tetrahedra (a) a brucite layer (b) and interlayer sites (c).

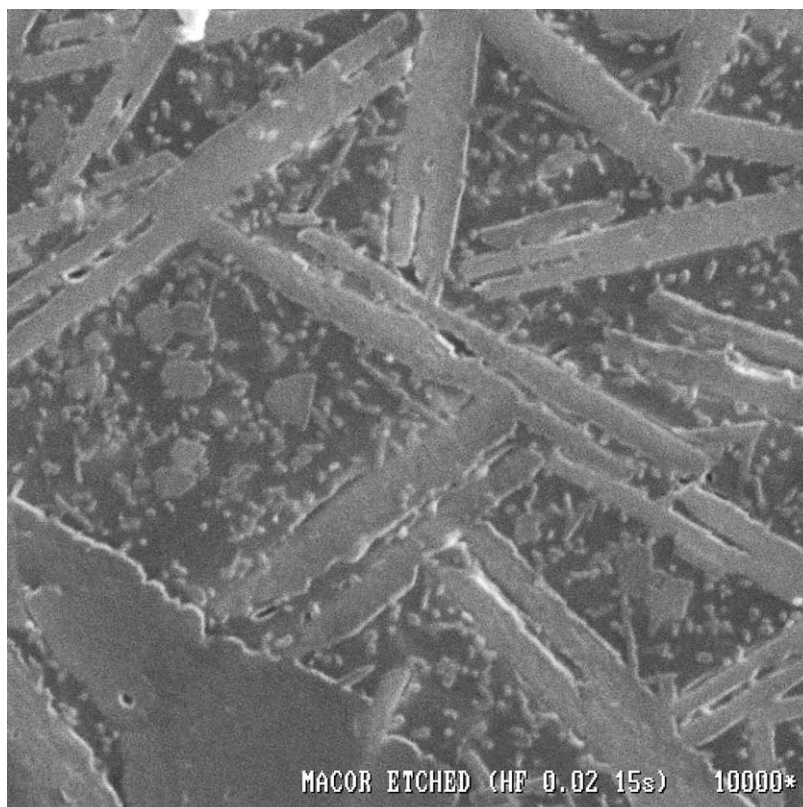


Figure 2 Microstructure of the commercial machinable glass-ceramic Macor based on a potassium fluorphlogopite glass-ceramic.

given. However it was stated that the compositions were close to the $Ba_{0.5}Mg_3(Si_3AlO_{10})F_2$ stoichiometry. They found improved strengths and also improved fracture toughness values. Addition of tricalcium phosphate $Ca_3(PO_4)_2$ was claimed to improve the stability of the glasses prior to crystallization.

Gregg and Anusavice [7, 8] in the USA have recently investigated microstructural development in one composition from the $Ca_3(PO_4)_2$ - $Ba_{0.5}Mg_3(Si_3AlO_{10})F_2$ - $Mg_2Al_4Si_5O_{18}$ system as part of a US NIH programme towards developing CAD CAM dental ceramics.

Currently most CAD CAM systems in the dental area use diamond tipped tooling and dental porcelains based on leucite ($K_2Al_2Si_4O_{12}$) as the ceramic material [9]. The leucite phase is very hard and abrasive. During

machining it causes tool wear and in clinical use it causes wear of the opposing teeth. An alternative system utilises a slightly modified DicorTM composition Dicor MGCTM based on a potassium tetrasilicic mica phase. The machinability of Dicor MGCTM and the dental porcelains is not ideal and they are prone to edge chipping during machining [10]. Furthermore for many applications both the dental porcelains and the Dicor MGCTM lack sufficient fracture toughness, with both materials having fracture toughness values in the range 1.0–1.40 $MPa\sqrt{m}$ [11]. Chipping and surface cracking of machined crowns and inlays adversely effects their strength [10]. What is required is a machinable ceramic with improved fracture toughness [11] preferably with a fracture toughness greater than that of dentine at 2.4 $MPa\sqrt{m}$.

1.1. Crystal phase development and microstructure

The MacorTM system is based on potassium fluorphlogopite $\text{KMg}_3\text{AlSi}_3\text{O}_{10}\text{F}_2$ crystals, whilst DicorTM and Dicor MGCTM are based on a tetrasilic mica, $\text{KMg}_{2.5}\text{Si}_4\text{O}_{10}\text{F}_2$.

The systems based on potassium fluorphlogopite are known to undergo a complicated crystallization sequence involving glass in glass, or amorphous phase separation to a magnesium rich matrix phase and an aluminium silicon rich droplet phase. This is then followed by crystallization of chondrodite $2\text{Mg}_2\text{SiO}_4\cdot\text{MgF}_2$, which crystallizes in the magnesium rich matrix at interface of the aluminium and silicon rich droplet phase. The chondrodite phase then transforms to norbergite $\text{Mg}_2\text{SiO}_4\cdot\text{MgF}_2$, which finally reacts with components in the residual glass phase to form potassium fluorphlogopite and a minor amount of mullite. The DicorTM system however nucleates directly probably via prior amorphous phase separation by a spinodal decomposition mechanism [12].

Machinability is thought to arise from the randomly orientated mica crystals with a house of cards structure allowing cracks to readily propagate between the mica planes, but hindering crack propagation across the layers (cards). It is thought that potassium micas cleave too easily giving rise to glass-ceramics with low fracture toughness. Replacing potassium ions with barium ions between the layers is thought to hinder cleavage and increases the fracture toughness.

Previous studies [13] have investigated compositions based on $8\text{SiO}_2\cdot 3\text{Al}_2\text{O}_3\cdot (6\text{-XMgO}\cdot\text{XMgF}_2\cdot\text{BaO})$, richer in silica and alumina compared to the stoichiometry of barium fluorphlogopite ($6\text{SiO}_2\cdot\text{Al}_2\text{O}_3\cdot(6\text{-XMgO}\cdot\text{XMgF}_2\cdot\text{BaO})$). These glasses failed to give the classic ‘‘house of cards’’ microstructure associated with machinability and this is thought to be a result of a residual glass phase that is rich in silicon and aluminium preventing the coarsening and growth of the barium fluorphlogopite crystal phase. A further disadvantage of these glasses is their tendency to crystallize to cordierite ($5\text{SiO}_2\cdot 2\text{Al}_2\text{O}_3\cdot 2\text{MgO}$) at the surface, following loss of volatile silicon tetrafluoride. Loss of silicon tetrafluoride reduces the fluorine content thereby reducing the amount of barium fluorphlogopite that can ultimately form and leaves a residual glass phase rich in silicon, aluminium and magnesium that is close to the cordierite stoichiometry and subsequently crystallizes to cordierite. Cordierite is an undesirable phase in a machinable glass-ceramic since it is hard and would result in increased tool wear. The commercial machinable glass-ceramic MacorTM is known to give rise to a hard surface layer up to 10 mm thick that has to be machined off prior to use. Glasses of lower alumina content were therefore studied in order to try and overcome these problems and in particular to produce compositions which do not crystallize to cordierite. This first part of this paper investigates the nucleation and crystallization behaviour, whilst the second part investigates how the microstructure, hardness and machinability are influenced by composition, heat treatment temperature and time.

TABLE I Y values, CLD, T_g and TEC values for the different aluminium oxide glasses studied

Glass code	Y value	CLD	Dilatometric T_g ($^{\circ}\text{C}$)	TEC ($\times 10^{-6} \text{ K}^{-1}$)
G1	3.50	1.23	640	6.21
G2	3.25	1.17	644	6.17
G3	3.00	1.11	632	6.67
G4	2.75	1.04	639	6.64
G5	2.50	0.96	640	6.39
G6	2.25	0.88	635	6.21
G7	2.00	0.79	629	6.58
G8	1.75	0.70	617	6.9
G9	1.50	0.59	607	7.07

2. Experimental

2.1. Glass synthesis

The glass-forming compositions studied are represented by the following generic formula:



Y was varied between 1.5 and 3.5 as shown in Table I. This compositional design also ensured that these compositions retained fluorine and that Lowenstein’s Aluminium Avoidance principle [14] was adhered to. N. H. Ray’s inorganic polymer model [15] of cross link density (CLD) was used to predict the properties of the glasses formed. The CLD values for these compositions are given in Table I. In addition the glasses were designed so that there was sufficient magnesium to ensure the formation of at least one non-bridging oxygen per silicon atom. The non-bridging oxygens are thought to preferentially bond to the silicon atoms present, thereby, preventing the formation of silicon-fluorine bonds and the formation of volatile silicon tetrafluoride.

The glasses were produced by melting silica, alumina, magnesium carbonate, magnesium fluoride and barium carbonate in high density mullite crucibles (Zedmark Refractories Earlsheaton Dewsbury UK) at a temperature of 1420°C for two hours. A batch size of approximately 800 g was used. The resulting melts were rapidly shock quenched into water to prevent phase separation and crystallization. The crucible and contents were weighed before and after firing. Weight losses were always less than one percent after allowing for loss of carbon dioxide. The glass frit produced was ground and sieved to give fine ($<45 \mu\text{m}$) and coarse ($45\text{--}200 \mu\text{m}$) particles, which were used in the subsequent analysis.

2.2. Glass characterization

2.2.1. Differential scanning calorimetry (DSC)

The glasses produced were characterized by differential scanning calorimetry using a Stanton Redcroft DSC 1500 (Rheometric Scientific, Epsom, UK) The crucibles used were matched pairs made of platinum-rhodium alloy. Alumina was used as the reference material. Runs were performed in dry nitrogen at a heating rate of $10^{\circ}\text{C min}^{-1}$ unless otherwise stated. The

tendency of the glasses to undergo surface nucleation was assessed by performing DSC runs using three particle sizes; frit particles of 1–2 mm, coarse of 45–200 μm and fine of <45 μm .

Optimum nucleation temperatures were determined using the method outlined by Marrotta [16] using one hour nucleation holds. Activation energies for crystallization were determined following nucleation holds at the previously determined optimum nucleation temperatures using the method outlined by Marrotta *et al.* [17] and the modified Kissinger method proposed by Matusita and Sakka [18].

The basis of the method developed by Marrotta *et al.* is:

$$\ln\beta = E_c/RT_p + \text{Constant.}$$

where β is the reciprocal of the heating rate, E_c is the activation energy of the process, T_p is the crystallization peak temperature and R the universal gas constant.

Whilst the modified Kissinger method developed by Matusita and Sakka is based on:

$$\ln(Tp^2/\beta^n) = -mE_c/RT_p + \text{Constant.}$$

where T_p is the temperature corresponding to the maximum of the crystallization peak, R is the gas constant, β is the heating rate and in the modified Kissinger n and m are the numerical constants, which depend on the crystallization mechanism. For the case of surface nucleation $n = m = 1$, whilst for bulk nucleation from a constant number of nuclei $n = m = 3$ whilst for bulk nucleation from an increasing number of nuclei $n = 4$ and $m = 3$.

These methods make the assumption that the glass composition does not change as crystallization proceeds, which is questionable with glasses, which are of different composition to the crystalline phase that forms. However the activation energies obtained from these methods often give some insights into the nucleation and growth processes involved. Assumptions also have to be made with the modified Kissinger method, about the appropriate values used for n and m . In some cases neither pure bulk nucleation or surface nucleation occur giving rise to non-integer values for n and m . Five heating rates of 2, 5, 10, 15 and 20 $^\circ\text{C min}^{-1}$ were used for the activation energy analysis.

2.2.2. Combined differential thermal analysis/thermal gravimetric analysis (DTA/TGA)

Combined DTA/TGA was used to study weight changes accompanying crystallization processes. A Stanton Redcroft DTA/TGA 1600 (Rheometric Scientific, Epsom, UK) was used with a flowing dry nitrogen atmosphere and a heating rate of 10 $^\circ\text{C min}^{-1}$.

2.2.3. Dilatometry

Sample rods measuring 4 mm \times 4 mm and 10 mm high were cast from frit and bars measuring 4 mm \times 4 mm

by 10 mm were cut from these rods for dilatometry. The thermal expansion coefficient (TEC) between 200 and 500 $^\circ\text{C}$ and the glass transition temperature were determined using a Netzch dilatometer (Netzch dil402) at a heating rate of 5 $^\circ\text{C min}^{-1}$.

2.2.4. X-ray powder diffraction

Five heat treatment temperatures were investigated by X-ray powder diffraction on frit and <45 micrometer samples. All samples were heat-treated using a ramp rate of 10 $^\circ\text{C min}^{-1}$ and then cooled. A Phillips powder diffractometer (Phillips Xpert diffractometer, Phillips Eindhoven NL) was used with Cu K_α X-rays. Every glass composition was heat treated using the tube furnace of the DSC to replicate the DSC analysis using an identical heating rate with samples taken at the individual crystallization temperatures for each glass.

3. Results and discussion

The synthesis of these glass compositions resulted in no significant silicon tetrafluoride volatilization during the melting of each batch of the glass and optically clear and homogeneous glasses were produced. There was no significant corrosion of the crucibles by any of the glass compositions studied. The amorphous nature of each glass was revealed by a single amorphous halo between 15 and 40 ($^\circ 2\theta$), from powder XRD of base glass samples.

Typical DSC traces are shown in Fig. 3. There is a clear glass transition temperature followed by two exothermic crystallization peaks termed T_{p1} and T_{p2} . These are followed by a sharp endotherm in the temperature range 1200 to 1260 $^\circ\text{C}$. Fig. 4 shows the glass transition temperature plotted against the alumina content of the glass Y . Aluminium will go into the glass network as a four coordinate ion and this requires an additional unit of positive charge to maintain charge neutrality. Reducing the alumina content results in some of the alkali earth cations switching their role from charge balancing Al^{3+} ions to forming non-bridging oxygens. There is a consequent increase in the disruption of the glass network and a fall in the calculated crosslink

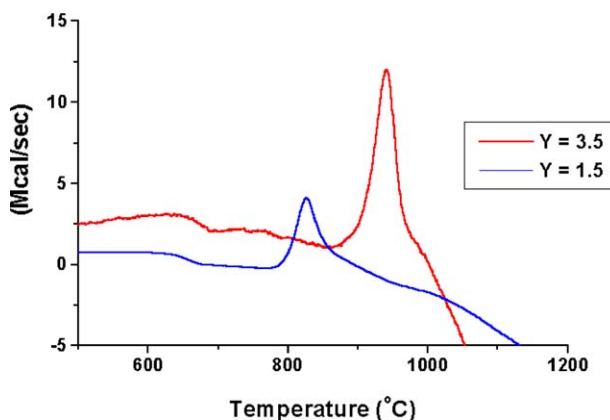


Figure 3 DSC trace for the $Y = 3.5$ and $Y = 1.5$ glasses showing the principal features. Note the endotherms are not shown for scaling reasons.

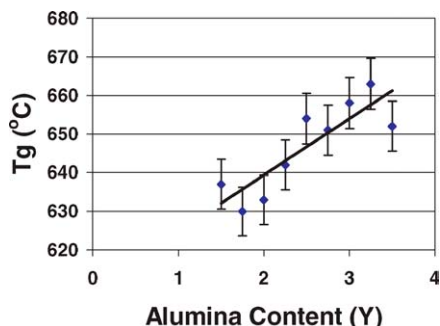


Figure 4 Glass transition temperature (T_g) obtained from DSC measurements plotted against alumina content (Y).

density values, resulting in the glass transition temperature reducing. There is a slight increase in the glass transition temperature for the lowest alumina content glass, which may be the result of a small amount of SiF_4 volatilisation which would be favoured by the low alumina content.

The thermal expansion coefficient (TEC) is shown in Table I along with the T_g values determined by dilatometry. The dilatometric T_g falls in line with the observed fall in the T_g determined by DSC. However the TEC does not change in a systematic way as the alumina content is varied.

A reduction in the alumina content of the glass also causes a reduction in the first peak crystallization temperature (T_{p1}). The results for frit and $<45 \mu\text{m}$ samples, are shown in Fig. 5. The values for T_{p1} for different glass particle sizes converge with reducing alumina content, indicating an increase in the tendency of the glasses to undergo bulk crystal nucleation. However, the main disadvantage of the reduction of alumina content appeared in its effect on the casting window (T_{p1} onset- T_g) for each glass composition. For example the casting window reduced from 215°C for G1 to 150°C for G9. The reduction of this window affects both the castability and the processibility of these materials. A small casting window would make it more difficult to control the casting of the glasses into homogeneous monoliths without prematurely crystallizing the glass.

The second crystallisation peak, T_{p2} is weak or absent for frit material and increases in magnitude with reducing particle size. The values for T_{p2} are shown in Fig. 6. The values for T_{p2} reduce with reducing alumina content. The amplitude of the T_{p2} peak reduced and eventually disappeared with a reduction in

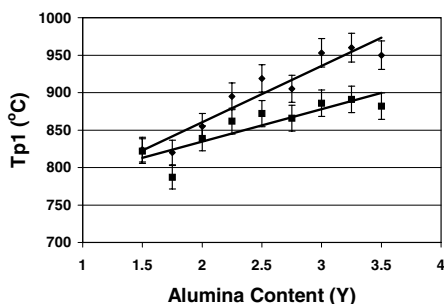


Figure 5 T_{p1} values for Δ Frit particles, \blacksquare = $<45 \mu\text{m}$ particles illustrating a reduction in T_{p1} with a reduction in aluminium content (Y).

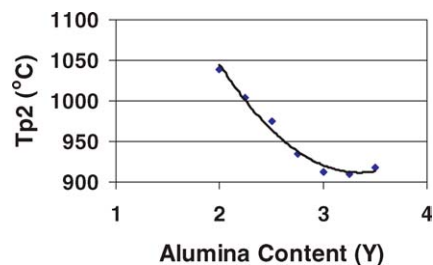


Figure 6 Second peak crystallization temperature plotted against alumina content (Y). Note the absence of T_{p2} for glasses with $Y > 2.0$.

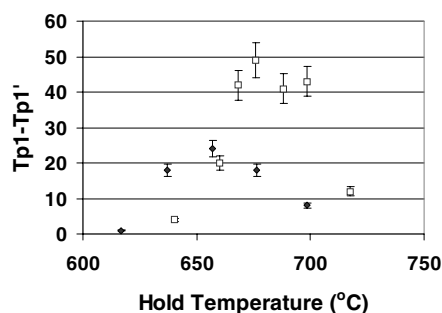


Figure 7 Optimum nucleation curves T_{p1} - T_{p1}' against nucleation hold temperature where T_{p1}' is the first peak crystallization temperature with a nucleation hold for $Y = 3.5$ (\square) and $Y = 1.5$ (\blacklozenge) glasses.

alumina content below $Y = 2$. It can be concluded that T_{p2} probably corresponds to a strongly surface nucleating alumina rich phase. It is likely to be cordierite, $5\text{SiO}_2 \cdot 2\text{Al}_2\text{O}_3 \cdot 2\text{MgO}$, an aluminium-containing phase that is favoured when significant silicon tetrafluoride volatilisation occurs.

These glasses also demonstrated melting endothermic peaks in the range 1230 to 1270°C . These endotherms became broader and are of reduced magnitude for lower alumina content glasses. Natural potassium phlogopites are known to melt or decompose in the temperature range 1150 to 1250°C with the melting temperature increasing with fluorine content [19]. The sharp melting endotherm at 1260°C present in the higher alumina content glasses is therefore thought to correspond to that of barium fluorphlogopite. The broader melting endotherms in the lower alumina content glasses are therefore thought to correspond to simultaneous melting of the residual glass phase and barium fluorphlogopite.

Typical optimum nucleation curves determined using the Marrotta method [16] are shown in Fig. 7 for the $Y = 3.5$, $Y = 2.5$ and $Y = 1.5$ glasses. Classic dome shaped curves are obtained. The optimum nucleation temperatures for all the glasses are also listed in Table II. In all cases the optimum nucleation temperature corresponded approximately to the midpoint of the glass transition and the dilatometric softening point of each glass composition. The formation of a new T_{p2} peak, as a result of the T_{p1} peak splitting into two crystallization peaks, was observed in compositions with high alumina contents $3.25 \geq Y \geq 2.5$. This new crystallization peak is only found when an isothermal hold is applied. A significant departure from a high alumina composition ($Y \geq 2.75$) reduces the formation of this

TABLE II Aluminium content, optimum nucleation temperatures glass transition temperatures and softening points

Y value	Optimum nucleation temperature (°C)	Tp1-Tp1 (°C)	T_g midpoint (°C)	Softening point (Dilatometry) (°C)
3.50	683	48	679	682
3.25	685	24	665	680
3.00	685	38	671	681
2.75	662	41	662	682
2.50	664	43	664	680
2.25	658	47	657	680
2.00	653	65	666	680
1.75	640	14	639	667
1.50	655	24	654	661

second crystallization peak, until it completely disappears in compositions with $Y \leq 2.25$.

An optimum nucleation temperature close to T_g [20] is indicative of a nucleation mechanism occurring via prior amorphous phase separation (APS). Supporting evidence for this nucleation route was provided by the observation that the formation of conventional precursor crystal phases, such as norbergite or chondrodite did not occur in heat-treated samples prepared for powder XRD. However the suspected APS nucleation route of these glasses was not significant enough to produce very favourable bulk crystallisation in all glasses, until Y was < 2 . It is thought that reducing the alumina content results in increased network disruption that allows the glass to undergo APS more readily.

Combined DTA/TGA revealed that weight loss was independent of composition, but was related to particle size. In fluoro-silicate and fluoro-alumino-silicate glasses the weight loss is known to be due to silicon tetrafluoride (SiF_4) volatilisation [21–24]. The weight loss increased with a reduction in particle size of the glass and hence an increase in surface area. The onset of significant weight loss was also shown to be at much higher temperatures corresponding to the onset of the observed endothermic transition for frit samples when compared to samples of $< 45 \mu\text{m}$ powder. This agrees with previous work conducted by Wood *et al.* [24] who showed the formation of proto-enstatite, $\text{SiO}_2\text{-MgO}$ a fluoride free crystal phase, on the surface of cast samples of DicorTM as a consequence of SiF_4 volatilisation.

Activation energies for crystallisation are given in Table III. The exponents n and m were assumed to be 3 and 3 corresponding to 3 dimensional growth from a fixed number of nuclei in the Matusita method. There is good agreement between the two methods used to calculate the activation energy for crystallisation. The activation energies are similar to those obtained by Bapna and Mueller for the DicorTM glass-ceramic who obtained a value of 203 kJmol^{-1} . The activation energy initially rises then falls then rises again with decreasing alumina content. It might have been expected that the activation energy would fall with reducing alumina content and increased network disruption since activation energies for crystallisation often correlate with those for viscous flow.

Some errors may be introduced in the activation energy determination in the high alumina-containing

TABLE III Activation energy values and the respective linear regression values for $8\text{SiO}_2(Y)\text{Al}_2\text{O}_3\text{3.75MgO} \cdot 2.25\text{MgF}_2\text{BaO}$ glasses

Y value	Marotta Tp1 (KJ/mol)	Linear fit R^2	Matusita Tp1 (KJ/mol)	Linear fit R^2
3.50	264	0.97	255	0.96
3.25	366	0.99	360	0.99
3.00	226	0.95	205	0.94
2.75	291	0.99	285	0.99
2.50	261	0.99	254	0.99
2.25	256	0.99	250	0.98
2.00	230	0.99	223	0.99
1.75	140	0.99	134	0.99
1.50	255	0.97	249	0.97

compositions, ($Y \geq 2.25$) as a result of the crystallization of a secondary crystal phase at Tp2 with heating rates of $15^\circ\text{C}/\text{min}$. or greater. The formation of the Tp2 peak is most likely facilitated by a low degree of crystallization at Tp1. Therefore, this would result in an alumina and silica-containing residual glass phase, which is compositionally closer to the phase that forms at Tp2. The formation of an alumina and silica phase, such as mullite, would be facilitated at this crystallization temperature.

Finally, the reason for the unusually low values of E_a Marotta and E_a Matusita calculated for $Y = 1.75$ are not clear. However, a the broad crystallization peak observed at Tp1 may indicate that two crystal phases are attempting to crystallize simultaneously. This behaviour would render the E_a values useless, because this form of investigation can only be conducted on composition with well-separated crystallization processes. The slight increase in E_a values for the $Y = 1.5$ composition may be indicative of a slight change in composition resulting from fluorine loss during glass synthesis.

The JCPDS reference files used to identify the various crystal phases formed are presented in Table IV. The results of the XRD analysis on different alumina-containing glasses are summarised in Table V. The formation of an apparent kinoshitalite ($\text{BaMg}_3\text{Si}_2\text{Al}_2\text{O}_{10}(\text{OH})_2$) phase is dominant in all heat treatments for frit and $< 45 \mu\text{m}$ samples, and the amount of this phase increases with increasing heat treatment

TABLE IV List of JCPDS files used to identify the main crystal phase formations observed

Crystal phase	JCPDS reference files
Kinoshitalite (K) $\text{BaMg}_3\text{Si}_2\text{Al}_2\text{O}_{10}(\text{OH})_2$	(43-0687) and (19-0117) Barium magnesium aluminium fluoride silicate $\{\text{BaMg}_3\text{Al}_2\text{Si}_2\text{O}_{10}\text{F}_2\}$
Cordierite (C) $\text{Mg}_2\text{Si}_5\text{Al}_4\text{O}_{18}$	(2-0303) and (13-0294) [(13-0293), (12-0235), (12-0244) and (2-0445): Indialite] and (39-0273): Ba-substituted indialite]
Mullite (M): $\text{Si}_2\text{Al}_6\text{O}_{13}$	(15-0776), (22-0018) and (38-0471) sillimanite Al_2SiO_5
Barium aluminum silicate (BAS) $\text{BaSi}_2\text{Al}_2\text{O}_8$	(26-0137)
Enstatite (E) MgSiO_3	(19-0768) and [(35-0610), (13-0415) and (19-0769): clinoenstatite MgSiO_3

TABLE V List of heat treatments and results of XRD analysis of alumina series $Z = 1$ compositions and crystal phase identification

Y value	Tp1	Tp2	1000°C	1100°C	1200°C
$Y = 3$ frit $<45 \mu\text{m}$	SK	SK	SK, WC	SK, MC, WE	SK, SC, WE
	SK		SK, WM	SK, SM, WB, WE	SK, SB, SE
$Y = 3.25$ frit $<45 \mu\text{m}$	SK	SK, MC	SK, MC, MM	SK, MC, MM, WE	SK, SC, WM, WE
	SK		SK, MC, WM	SK, SC, WM	SK, WM, SB, SE
$Y = 3$ frit $<45 \mu\text{m}$	SK	SK	SK, WC, WM	SK, MC, SM	SK, SC, SM
	SK		SK, WC, MM	SK, WC, MM	SK, SC, WM, MB
$Y = 2.75$ frit $<45 \mu\text{m}$	SK	SK	SK, WC, MM	SK, WC, MM	SK, MC, SM
	SK		SK, WM	SK, MM	SK, SB, SE
$Y = 2.5$ frit $<45 \mu\text{m}$	SK	SK	SK	SK, MC	SK, WC, SM
	SK		SK	SK, WM, ME	SK, SB, SE
$Y = 2.25$ frit $<45 \mu\text{m}$	SK	SK	SK	SK	SK, MC, W??
	SK		SK		SK, SB, SE
$Y = 2$ frit $<45 \mu\text{m}$	SK	SK	SK	SK	SK, WC, W??
	SK		SK	SK, WC, WE	SK, SB, SE
$Y = 1.75$ frit $<45 \mu\text{m}$	SK	SK	SK	SK	SK
	SK		SK	SK, WB, WE	SK, SB, SE
$Y = 1.5$ frit $<45 \mu\text{m}$	SK	SK	SK	SK	SK
	SK		SK	SK, WB	SK, MB, SE

(S = Strong, M = Medium, W = Weak, K = Kinoshitalite, C = Cordierite, B = Barium Aluminium Silicate, M = Mullite, E = Enstatite and ?? = Unknown)

temperature, as can be seen in Fig. 8. However, analogous with the results of a previous study [13] the crystallization of secondary phases rich in alumina and silica and containing no fluorine, such as cordierite, mullite and barium aluminium silicate (BAS), are formed at high temperatures ($>1100^\circ\text{C}$). However, due to the dependence of these phases on alumina the proportions of these phases reduce with the alumina content of the glass. Examples of the successive reduction of these secondary phases can be seen from the reduction in the amount of cordierite in frit samples (Fig. 9) and from the reduction of BAS in $<45 \mu\text{m}$ samples (Fig. 10).

A significant reduction in the formation of cordierite occurs as the alumina content is reduced. This is observed by the reduction of its principal diffraction line at $10.5^\circ(2\theta)$. The significant suppression of cordierite formation occurs in compositions with $Y \leq 2$. As previously discussed [13], the formation of this crystal

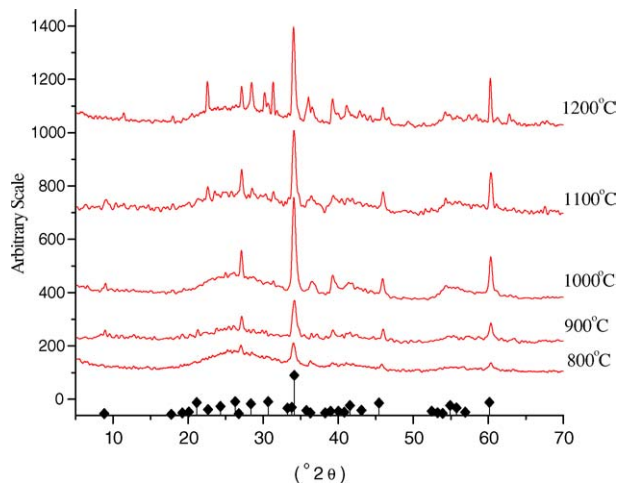


Figure 8 X-ray powder diffraction patterns of $<45 \mu\text{m}$ samples of the $Y = 1.5$ glass ($8\text{SiO}_2 (Y)\text{Al}_2\text{O}_3 3.75\text{MgO} 2.25\text{MgF}_2 \text{BaO}$) which illustrates the increased precipitation of Kinoshitalite \blacklozenge $\text{BaMg}_3\text{Si}_2\text{Al}_2\text{O}_{10}(\text{OH})_2$, 43-0687) with increasing temperature. (XRD patterns are spaced along the y-axis for the purposes of clarity).

phase is influenced by the decomposition/loss of the barium fluorophlogopite phase. The crystallization of cordierite is most significant at the onset to the major endotherm at 1260°C . The absence of this crystal phase from the $<45 \mu\text{m}$ samples indicates that the formation of cordierite is inhibited by crystallization of BAS, mullite and enstatite.

The formation of a mullite crystal phase is initially observed at approximately 1000°C in glasses with $Y \geq 2.5$. and it is favoured by the high alumina and silica content available in these compositions.

The reduction in the formation of BAS can also be observed by the reduction of its principal diffraction line at approximately $30^\circ(2\theta)$, as shown in Fig. 10. However, only a significant reduction of the amount of

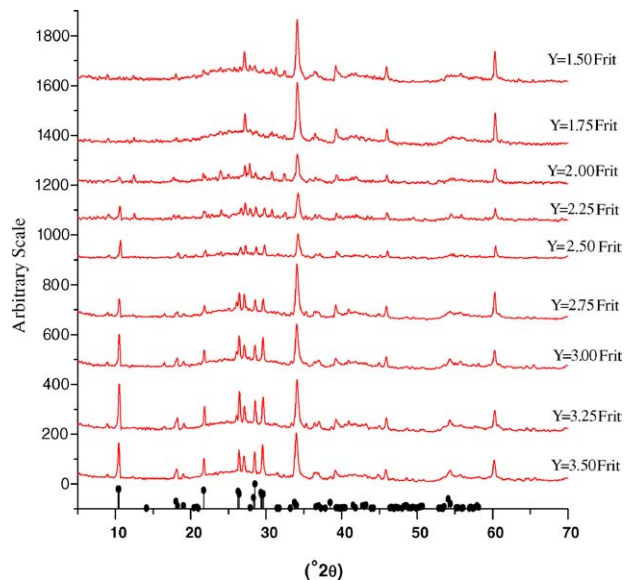


Figure 9 X-ray powder diffraction patterns for frit samples of various alumina (Y value) containing compositions ($8\text{SiO}_2 (Y)\text{Al}_2\text{O}_3 3.75\text{MgO} 2.25\text{MgF}_2 \text{BaO}$) show a reduction in the amount of cordierite \bullet , $\text{Mg}_2\text{Si}_5\text{Al}_4\text{O}_{18}$) formed after a heat treatment to 1200°C . (XRD patterns are spaced along the y-axis for the purposes of clarity).

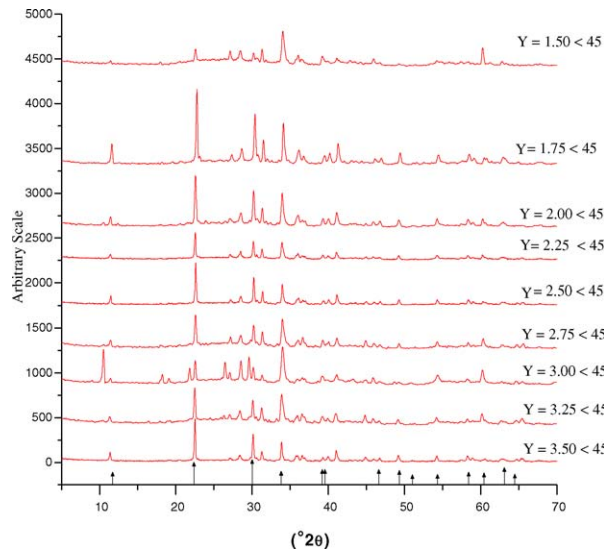


Figure 10 X-ray powder diffraction patterns showing the suppression of the BAS crystal phase \blacktriangle , $\text{Ba}_2\text{Si}_2\text{Al}_2\text{O}_8$) formation at 1200°C in $<45\ \mu\text{m}$ samples (8SiO_2 (Y) Al_2O_3 3.75MgO 2.25MgF_2 BaO) as a function of different alumina contents. (XRD patterns are spaced along the y-axis for the purposes of clarity).

this crystal phase is achieved with a $Y = 1.5$ alumina-containing composition.

BAS appears to form by a surface crystallization process, as this crystal phase is formed on a large scale in $<45\ \mu\text{m}$ samples only. Nevertheless, this phase is not likely to be associated with a direct surface crystallization process as this phase only crystallizes at high temperatures ($\geq 1100^\circ\text{C}$). Its formation is probably assisted by the decomposition of the barium fluorophlogopite phase. The BAS phase forms at the onset of the high temperature endotherm associated with the melting of a crystal phase (narrow endothermic peak). The reduction in magnitude of the endotherm with a reduction in alumina content correlates with a reduction in the formation of this phase. Therefore, the formation of this secondary crystalline phase is probably facilitated by fluorine loss, which results in a phase composition close in stoichiometry to BAS, which can be suppressed by a reduction of the alumina content.

The formation of a small amount of enstatite in addition to cordierite, as shown in Fig. 11, is observed in all composition of series D. The principal diffraction line of enstatite at $30.5^\circ(2\theta)$ is clearly present in addition to most of the weaker diffraction lines. The crystallization of this phase is most significant at high temperatures ($\geq 1200^\circ\text{C}$) close to the major melting endotherm at 1260°C . Its formation is a result of the melting of the apparent kinoshitalite phase in the $<45\ \mu\text{m}$ samples only, which is assisted by the large surface area of this small particle size.

X-ray diffraction (XRD) was conducted on frit and $<45\ \mu\text{m}$ samples (Fig. 12). Samples heat treated to Tp1 and above illustrate an almost complete depletion of the principal diffraction line of fluorophlogopite at approximately $9^\circ 2\theta$ corresponding to the interlayer spacing. Hoda and Beall [5] describes this phenomenon as “ionic disordering” of the interlayer crystal sites. In comparison with the potassium containing fluorophlogopites, a

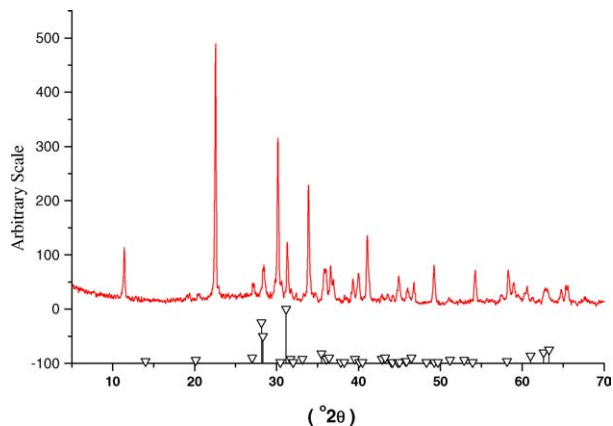


Figure 11 X-ray powder diffraction patterns of $<45\ \mu\text{m}$ samples for the $Y = 3.5$ composition (8SiO_2 (Y) Al_2O_3 3.75MgO 2.25MgF_2 BaO) which illustrates the formation of enstatite ∇ , magnesium silicate, MgSiO_3 , 19-0768) after a heat treatment to 1200°C .

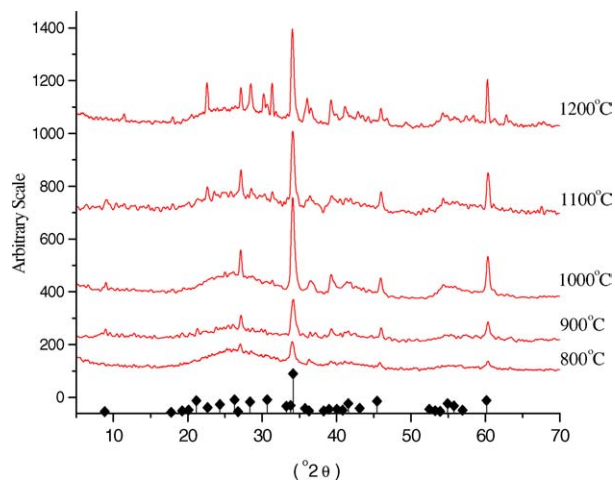


Figure 12 X-ray powder diffraction patterns for $<45\ \mu\text{m}$ samples of the $Y = 1.5$ glass (8SiO_2 (Y) Al_2O_3 3.75MgO 2.25MgF_2 BaO) which illustrates the increased precipitation of Kinoshitalite \blacklozenge $\text{BaMg}_3\text{Si}_2\text{Al}_2\text{O}_{10}(\text{OH})_2$, 43-0687) with increasing temperature. (XRD patterns are spaced along the y-axis for the purposes of clarity).

slight shift of the principle diffraction line would be expected to occur, as a result of the substitution of a slightly larger interlayer cation. The substitution of one barium cation for 2 potassium cations is stoichiometrically correct, and has been discussed by Eppler [25]. Curved fluorophlogopite crystals have been observed in mica glass-ceramics based on glasses with alumina contents in excess of the fluormica stoichiometry [26]. The reason for the curved micas crystals is thought to be lattice disordering associated with the substitution of magnesium for aluminium in the octahedral sites. This causes a rotation of the tetrahedral sheet about its c -axis, and subsequently a reduction these tetrahedral layers. However, this misalignment within the layered packets causes a shift of the principal peak to $10.6^\circ(2\theta)$, not its almost complete depletion. In a related study [27] the formation of a disordered barium fluorophlogopite crystal phase in these glasses was studied using Si^{29} MAS-NMR spectroscopy. Samples were examined based on frit and $<45\ \mu\text{m}$ samples heat-treated to Tp1. These materials illustrated the formation of a barium fluorophlogopite phase with respect to all frit

samples investigated. The main peaks of the fluorophlogopite spectra were at -86.3 , -88.7 and -92.1 ppm and agreed with previous studies [28, 29]. These peaks are associated with Q3[2Al], Q2[1Al] and Q3[0Al] co-ordinations. Minor spectral peaks were observed at -79.8 , -99.8 and -172.9 that correspond with a cordierite crystal phase. The $<45 \mu\text{m}$ samples also illustrated a barium fluorophlogopite phase together with an increased amount of cordierite, supporting previously discussed evidence for surface crystallisation of the latter phase due to volatilisation of SiF_4 from the surface and redissolution of the fluorophlogopite.

Higher heat treatment temperatures resulted in more barium fluorophlogopite being formed and also resulted in a sharpening of the diffraction lines. SEM showed the barium fluorophlogopite crystals to be greater than about one micron before the observed sharpening of the diffraction lines occurred. The sharpening of the diffraction lines is therefore likely to be due to the formation of a more ordered, less defective crystal structure with increasing heat treatment temperature.

4. Conclusions

Reducing the alumina content reduces the glass transition temperature, first peak crystallization temperature and promotes bulk crystal nucleation. Optimum nucleation temperatures were found to be close to the glass transition temperature indicating a possible nucleation route occurring via prior amorphous phase separation. The first peak crystallization temperature was shown to correspond to the crystallization of barium fluorophlogopite. No precursor crystal phases were found prior to the formation of barium fluorophlogopite. High alumina contents favoured the formation of cordierite, mullite and barium aluminium silicate. The second peak crystallization temperature reduced in magnitude with reducing alumina content and finally disappeared for compositions with low alumina contents.

The activation energy for crystallization varied from between 366 and 134 kJmol^{-1} but there was no correlation with alumina content.

Acknowledgements

The authors would like to acknowledge the financial support of the EU in the form of a Brite EuRam Contract BRPR-CT97-0521.

References

1. G. H. BEALL, in "Advances in Nucleation and Crystallization in Glasses," edited by L. L. Hench and S. W. Frieman (Amer. Cer. Soc., Westerville, 1971) p. 251.
2. C. K. CHYUNG, G. H. BEALL and D. G. GROSSMAN, in "Microstructure and Mechanical Properties of Mica Glass-Ceramics in Electron Microscopy and Structure of Materials," edited by G. Thomas, R. M. Fulrath and R. M. Fisher (Bekely University of California Press, 1972) p. 1167.
3. C. K. CHYUNG, G. H. BEALL and D. G. GROSSMAN, "Fluorophlogopite Mica Glass-Ceramics, 33–40," in Proc. International Glass Congress No. 14 Kyoto, Japan (Ceramic Society of Japan, Tokyo, Japan, 1974).

4. X. CHEN, D. LU, S. ZHAI, L. TENG, M. ZHANG and X. ZHANG, in "Research on the Mechanism of Phase Separation, Nucleation and Crystallization of Fluorophlogopite and Fluorapatite Containing Glass-Ceramics, Advanced Materials 93 II Biomaterials, Organic and Intelligent Materials," edited by H. Aoki *et al.* (Trans. Mat. Res. Soc., Japan, 1994) vol. 15A, p. 37.
5. S. N. HODA and G. H. BEALL, in "Alkaline Earth Mica Glass-ceramics," edited by J. H. Simmons, D. R. Uhlmann and G. H. Beall Advances in Ceramics: Nucleation and Crystallisation in Glasses. (J. Amer. Ceram. Soc., 1982) vol. 2, p. 287.
6. T. UNO, T. KASUGA and K. NAKJIMA, *J. Amer. Ceram. Soc.* **74** (1991) 3139.
7. J. A. GRIGGS and K. J. ANUSAVICE, *J. Dent. Res.* **75**(66) (1996) Abstract 389.
8. T. J. HILL, J. J. MECHOLSKY and K. J. ANUSAVICE, *J. Dent. Res.* **75**(66) Abstract no. 388.
9. J. VAN DER ZEL, *Prothodontics Quintessence Int.* **24** (1993) 769.
10. A. GRAF, J. SINDEL, R. FRANKENBERGER, P. GREIL and A. PETSCHL, Fracture Strengths and Fatigue Limits of CAD-CAM Machined Dental Ceramics, in "Proceedings of the Conference Clinically Appropriate Alternatives to Amalgam Biophysical Factors in Restorative Decision Making" (Academy of Dental Materials, 1996) p. 6, 236.
11. R. R. SEGHI and S. F. ROSENTIEL, *J. Prosthetic Dentistry*, August (1995).
12. M. S. BAPNA and H. J. MUELLER, *Biomaterials* **17** (1996) 2045.
13. J. HENRY and R. G. HILL (submitted to *J. Amer. Ceram. Soc.*).
14. W. LOWENSTEIN, *Amer. Miner.* **39** (1954) 92.
15. N. H. RAY, "Inorganic Polymers" (Academic Press, London, 1978).
16. A. MARROTTA, A. BURI and F. BRANDA, *J. Mater. Sci.* **16** (1981) 341.
17. K. MATUSITA and S. SAKKA, *J. Non. Cryst. Solids* **38** (1980) 741.
18. K. MATUSITA, S. SAKKA and Y. MATSUI, *J. Mater. Sci.* **10** (1975) 961.
19. G. H. BEALL, Mica Glass-Ceramics, US patent no. 3,689,293 (1972).
20. P. W. MCMILLAN, "Glass-Ceramics" (Academic Press, New York, 1979).
21. R. G. HILL, C. GOAT and D. WOOD, *J. Amer. Ceram. Soc.* **75** (1992) 778.
22. A. RAFFERTY, A. CLIFFORD, R. HILL, D. WOOD, B. SAMUNEVA and M. DIMITROVA-LUKACS, *ibid.* **83** (2000) 2333.
23. A. CLIFFORD, R. G. HILL, M. J. TOWLER and D. J. WOOD, *J. Mater. Sci.* **36** (2001) 461.
24. D. J. WOOD, N. L. BUB, A. CLIFFORD, R. HILL and J. C. KNOWLES, *J. Mater. Sci. Letts.* **18** (1999) 1001.
25. R. A. EPPLER, J. F. MACDOWELL and J. D. STETLER, Method of Making Crystalline Mica Bodies and Product. U.S. patent no. 3,149,947 (1964).
26. W. GÖTZ, G. PEITER, K. MIEHE and G. HOPFE, in "Forming of Curved Phlogopite-Crystals in Glass-Ceramic Material," edited by B. Samuneva, I. Gutzow, Y. Dimitriev and S. Bachvarov, 11th Conference on Glass and Ceramics. Proceedings, Varna, October 25–27, 1993. Sofia: "Marin Drinov" (Academic Publishing House, Sofia, 1993), p. 74.
27. N. DUNLEA, "Preparation and Structural Study of a Series of Mica-Based Glass-Ceramics," MSc. Thesis, National University of Ireland, Cork, 2000.
28. S. KOMARNENI, A. FYFE, G. J. KENNEDY and H. STROBL, *J. Amer. Ceram. Soc.* **69** (1986) C45.
29. S. CICONE, A. NAVROTSKY, R. J. KIRKPATRICK and C. M. GRAHAM, *Amer. Miner.* **76** (1991) 1485.

Received 19 April 2002

and accepted 1 October 2003